Article

Measuring the Efficiency of Raman Photoexcitation of Singlet Oxygen in Distilled Water

Aristides Marcano Olaizola *

Posted Date: 31 July 2025

doi: 10.20944/preprints202507.2572.v1

Keywords: Raman spectroscopy; singlet oxygen photoexcitation; efficiency of the Raman generated singlet oxygen

 doi:10.20944/preprints202507.2572.v1

Article

Measuring the Efficiency of Raman Photoexcitation of Singlet Oxygen in Distilled Water

Aristides Marcano Olaizola

Division of Physics, Engineering, Mathematics, and Computer Science, Delaware State University, 1200 North DuPont Highway, Dover, DE 19901, USA; amarcano@desu.edu; Tel.: 001 302 857 6690

Abstract

We determine the efficiency of singlet oxygen generated through a Raman excitation process in aerated distilled water. Focused nanosecond light pulses in the spectral blue region induce Raman transition toward the singlet oxygen state, generating a Stokes signal in the red spectral region. The signal is proportional to the number of photons corresponding to the amount of excited oxygen molecules. We calculate the efficiency by dividing the number of generated singlet oxygen molecules by the number of incoming pumping photons. We determine an efficiency of (8±2) 10^{-5} for water when pumping at 410 nm with a pulse energy of 13 mJ. We demonstrate that the Raman method exhibits no photobleaching, a phenomenon typically observed when photosensitizers are used. Thanks to this property, Raman excitation continues as long as the sample is irradiated, generating more singlet oxygen molecules over time than the photosensitization method.

Keywords: Raman spectroscopy; singlet oxygen photoexcitation; efficiency of the Raman generated singlet oxygen

1. Introduction

Singlet oxygen ($^1O_2$) corresponds to the lowest excited electronic quantum level of molecular oxygen. In this state, the molecule is highly electrophilic, which is the basis for its broad applications in photochemistry, photobiology, and photomedicine [1-5]. Quantum mechanics forbids direct one-photon excitation toward the $^1O_2$ state, resulting in a low transition probability. Photosensitization is the general method for efficient $^1O_2$ photoproduction [6-7]. A large photosensitizer molecule absorbs visible (VI) light, accumulating the absorbed energy on a triple metastable level. From there, the energy is transmitted to surrounding oxygen molecules, exciting the $^1O_2$ state. We have recently demonstrated a photosensitizer-free $^1O_2$ photoexcitation based on the Raman effect [8-10]. A pumping photon produces a Raman transition from ground toward the $^1O_2$ level, emitting a Stokes photon of lower energy. The difference between the pumping and Stokes photon energies is equal to the energy needed for the transition. The lack of use of the photosensitizer simplifies the procedures and prevents potential secondary effects, like excessive photosensitivity or unexpected phototoxicity. In a recent publication, we demonstrated the detection of phosphorescence at 1270 nm from the Raman photoexcited $^1O_2$ [10]. However, determining the efficiency of the process (Φ_Δ) is still a task to be completed. The present work eliminates the gap. We define Φ_Δ as the relation between the number of Raman-generated $^1O_2$ molecules and the total number of pumping photons. We measure Φ_Δ of (8±2) 10^{-5} in distilled water (H_2O) when pumping at 410 nm with nanosecond pulses of an energy of 13 mJ.

Furthermore, we compare the Raman approach with the photosensitization method using the well-known photosensitizer, Rose Bengal. The $^1O_2$ chemical trap, uric acid, is used to evaluate both methods. We show that, over time, the Raman method generates more $^1O_2$ molecules than the photosensitization method. Rose Bengal exhibits near-full photobleaching after sixty minutes of irradiation, interrupting $^1O_2$ photoproduction. In the Raman method, photobleaching does not take place. Consequently, the Raman $^1O_2$ generation continues without interruption even after hours of irradiation.

 doi:10.20944/preprints202507.2572.v1

2. Theoretical Considerations

Figure 1a shows a simplified schematic of $^1O_2$ Raman excitation. A pumping photon induces a Raman transition from the ground toward the $^1O_2$ level, emitting a Stokes photon. For example, when pumping at 410 nm in H_2O, the $^1O_2$ Stokes component occurs around 605 nm. The magnitude of this signal yields a direct measurement of the amount of excited $^1O_2$ molecules. Other Stokes photons related to the excitation of solvent vibrational modes and their overtones are generated. When pumping at 410 nm, the H_2O stretching vibrational mode produces a Stokes component at 475 nm. An additional overtone of this Stokes signal is also observed at 566 nm. The difference in wavelength between the Stokes components allows for their identification and separation using optical filters. Experiments below demonstrate that most of the energy involved in the Raman process originates from the solvent stretching modes. Despite this fact, the $^1O_2$ Stokes can still be detected, showing that a significant amount of $^1O_2$ molecules is still being generated.

In the photosensitization method, the photosensitizer's quantum yield measures the efficiency of $^1O_2$ photoproduction [11-15]. The photosensitizer's quantum yield is defined as the number of excited oxygen molecules divided by the number of photons absorbed by the photosensitizer. The commonly used photosensitizer Rose Bengal exhibits a quantum yield value of 0.76 at 532 nm in H_2O [15-16]. As discussed above, for the Raman method, Φ_Δ is defined by the equation

$$\Phi_\Delta = \frac{N_\Delta}{N_p}, \qquad (1)$$

where N_Δ and Np are the number of $^1O_2$ Stokes and pumping photons, respectively. The number of photons can be estimated by measuring the signal energy corresponding to each process divided by the energy of one photon. Then, we can write

$$\Phi_\Delta = \frac{\bar{\lambda}_\Delta g E_\Delta}{\lambda_p o E_p}, \qquad (2)$$

where $\bar{\lambda}_\Delta$ is the averaged $^1O_2$ Stokes wavelength, E_Δ is its energy, λ_p is the pump wavelength, and E_p is its energy.

2. Materials and Methods

Figure 1b shows the experiment setup. An optical parametric oscillator (OPO, OPOTEK, Carlsbad, CA, US) provides 6-nanosecond excitation in the blue-green region (410-520 nm) with an average energy per pulse of 14 mJ. A beam splitter B deviates part of the light toward a reference detector. A 20 cm focal length lens L_1 focuses the pump light onto a 10 cm path-length glass cuvette containing the sample. A neutral filter (NDF1) placed at the exit of the sample significantly reduces the power to avoid optical damage to the filters. A lens L_2 focuses the resulting signal onto the detector. An additional neutral density filter, NDF2, is placed at the entrance of the detector, reducing the signal intensity to avoid detector saturation. To detect the signal, we use a silicon detector (Thorlabs DET100A2, Newton, NJ, US) with a responsivity of 0.2 A/W at 410 nm and 0.4 A/W at 610 nm and a rise time of 35 ns.

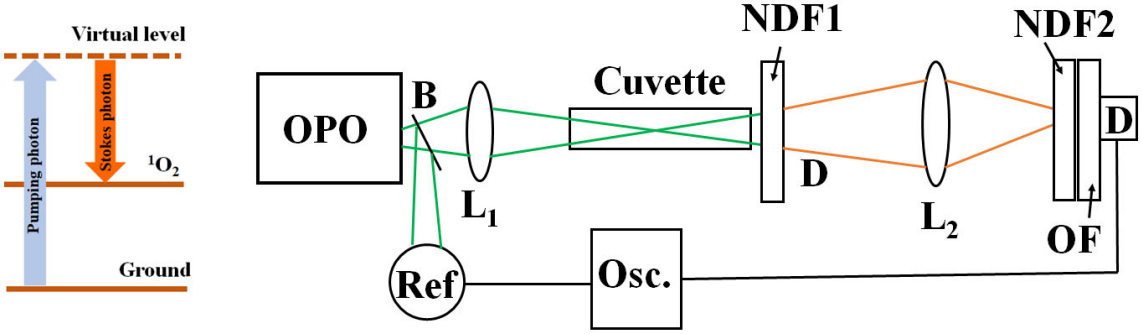

 doi:10.20944/preprints202507.2572.v1

(a) (b)

Figure 1. (a) Schematic of the Raman excitation of oxygen dissolved in the solvent. (b) Experimental setup showing the optical parametric oscillator (OPO), a beam splitter B, a reference detector Ref, lenses L_1 and L_2, the sample cuvette, neutral density filters NDF1 and NDF2, an optical filter OF, a silicon detector D, and an oscilloscope.

The silicon detector signal is sent without further amplification toward a digital oscilloscope (TDS 3052, Tektronix, Beaverton, OR, US) for averaging and display. The oscilloscope averages 512 pulses, providing a stable signal proportional to the emitted luminescence. Due to their Raman character, the Stokes signals follow the time dependence of the pump pulse. Since the detector risetime is longer than the excitation pulse, the signal time evolution is limited by it. To calibrate the signal provided by the silicon sensor, we use calibrated detectors. To measure pulse energies above 100 µJ, we use a pyroelectric energy meter (PE25BF-DIF-C, Ophir USA, Newport Corporation, North Logan, UT, US). For measuring energies below 100 µJ, we use a diode power meter (Thorlabs PM100, Newton, NJ, US).

We detect the pump signal using the corresponding interference filter. When pumping at 410 nm, we use an interference filter at (410±10) nm. The $^1O_2$ Stokes signal is measured using a long-pass filter. When pumping at 410 nm, we use a filter with a cutoff at 610 nm. Below, we show that the collected signal corresponds to the amount of $^1O_2$ molecules. The Stokes signals from the solvent stretching modes are evaluated in a similar manner.

Aerated distilled H_2O in 20 cm and 10 cm pathlength glass cuvettes was used as a sample. We use solutions of sodium bisulfite ($NaHSO_3$) as an oxygen quencher to aid in identifying the oxygen contribution [17]. The concentration of dissolved oxygen in H_2O decreases when the $NaHSO_3$ concentration increases. Water solutions of $NaHSO_3$ exhibit a reduced $^1O_2$ Stokes signal, as it corresponds to a reduced oxygen concentration. To measure the amount of oxygen in the solutions, we used an oxygen optical sensor (Vernier Optical DO Probe, Vernier, Beaverton, OR).

We used uric acid as a $^1O_2$ chemical trap to compare the efficiency of the photosensitization and Raman methods. The uric acid UV absorbance at 294 nm is a direct measurement of the amount of $^1O_2$ being generated [18-19]. We use Rose Bengal as a photosensitizer. A solution of 10 µM Rose Bengal in H_2O was prepared.

To collect spectra of the Stokes signals, we use a spectrometer (red Tide USB 650, Ocean Optics, Orlando, FL).

4. Results and Discussion

The solvent Stokes contributions are significant, but they can be eliminated using optical filters. Figure 2a shows the spectra collected using the Ocean Optics spectrometer after passing through neutral filters with a total optical density of six when pumping distilled water at 410 nm. The first peak at 410 nm corresponds to the pumping field. The peak at 475 nm corresponds to the H_2O stretching mode at a frequency of 3350 cm^{-1} [20-23]. This mode is the dominant part of the total Stokes field.

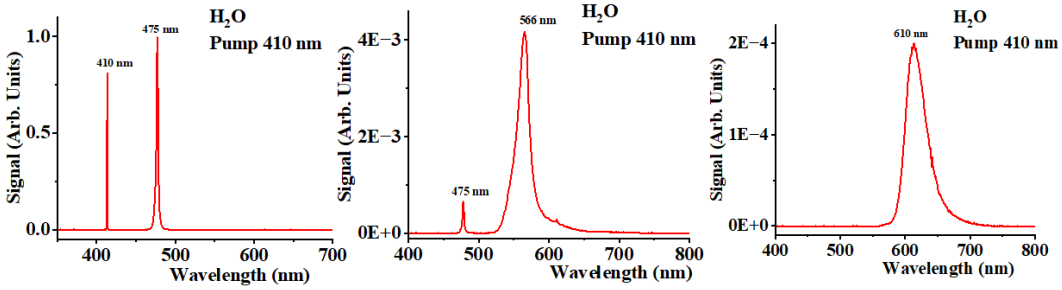

 doi:10.20944/preprints202507.2572.v1

(a) (b) (c)

Figure 2. (a) Raman spectra obtained using neutral filters with an optical density of six. (b) Raman spectra obtained using a neutral density filter with an optical density of two and a longpass filter with a cutoff at 550 nm. (c) Raman spectra obtained using neutral density filters with an optical density of one and a long-pass filter with a cutoff at 610 nm.

Figure 2b shows the spectrum after using a neutral density filter with an optical density of two and a long-pass filter with a cutoff at 550 nm. A diminished Stokes peak at 475 nm and a peak at 566 nm are observed. The last peak corresponds to the first overtone of the H_2O vibrational mode at 6700 cm^{-1}. When using a neutral density filter with an optical density of one and a long-pass filter with a cutoff at 610 nm, the solvent Stokes components at 475 nm and 566 nm are fully depleted (see Figure 2c). The arbitrary units in all figures (2a, 2b, and 2c) are the same. Thus, the signal depicted by Figure 2c is four orders of magnitude smaller than the signal shown on Figure 2a and one order of magnitude smaller than the signal shown on Figure 2b. To demonstrate that the curve shown in Figure 2c is oxygen-dependent, we reduce the oxygen concentration using the oxygen quencher $NaHSO_3$.

Figure 3a shows the singlet peak obtained when using the long-pass filter at 610 nm for different concentrations of $NaHSO_3$. The blue line corresponds to the condition where no $NaHSO_3$ is added. As the $NaHSO_3$ concentration increases, the signal decreases. At a concentration of 40 mg/ml, the signal has been significantly reduced. Using the optical oxygen sensor, we measure the oxygen concentration in each sample solution. Figure 3b shows how the oxygen concentration decreases as the $NaHSO_3$ concentration increases. A nearly linear dependence is observed for concentrations below 10 mg/ml. Figure 3 shows that the observed Stokes signal collected using the 610 nm long-pass filter is oxygen-dependent. Its amplitude provides a direct measurement of the amount of $^1O_2$ molecules being generated in the process. We note that the H_2O Stokes components are not affected by the presence of $NaHSO_3$.

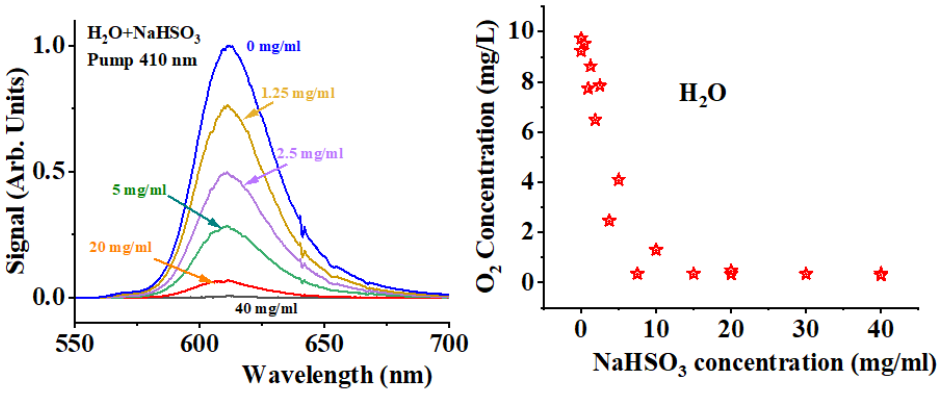

(a) (b)

Figure 3. (a) $^1O_2$ Stokes spectra for solutions of $NaHSO_3$ in H_2O at different concentrations. (b) Oxygen concentration as a function of $NaHSO_3$ concentration. .

Figure 4a shows the pulse energy corresponding to the excitation pump light (blue light). The signal was collected using the diode detector and energy sensor for calibration purposes. We use an interference filter at (410±10) nm to select only the pump light. Using an interference filter at (475±10) nm, we collect a Stokes signal corresponding to the H_2O stretching mode at 3350 cm^{-1} (red line in figure 4a). A significant portion of the pump field, (23±1) %, is converted into this Stokes component. The standard deviation is estimated over 10 experiments. We also measured the contribution from the overtone at 566 nm using the corresponding filter, which accounted for (0.25±0.01) % of the total incoming light. The $^1O_2$ Stokes contribution is significantly smaller. Figure 4b shows the $^1O_2$ Stokes signal, together with the pumping signal, on a logarithmic scale. We estimated a pulse energy of

 doi:10.20944/preprints202507.2572.v1

(0.7±0.2) μJ. Under these conditions, equation (2) provides Φ_Δ=(8±2) 10^{-5}. Using these values, we estimate that each pulse of pumping light generates approximately 4 10^{11} $^1O_2$ molecules.

To understand the potential practical applications of the Raman method, we compare it with the conventional photosensitization method. We use the well-known photosensitizer Rose Bengal for this purpose. We prepare solutions of Rose Bengal in H_2O at a concentration of 10 μM. We also use uric acid at a concentration of 120 μM as a $^1O_2$ chemical trap to monitor the amount of $^1O_2$ being generated in each method. We irradiate the Rose Bengal and uric acid solution at 532 nm in five-minute intervals. At the end of each interval, we measure the UV spectrum of the solution to monitor the amplitude of the peak at 294 nm.

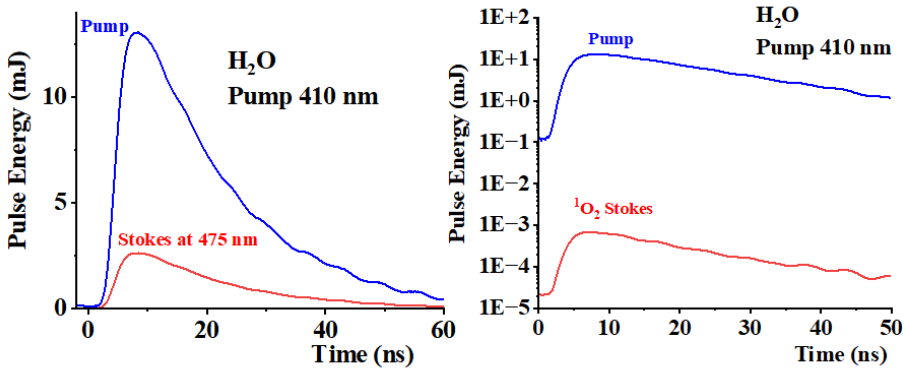

(a) (b)

5. Conclusions

We have estimated the efficiency of the $^1O_2$ Raman photogeneration in H_2O by measuring the signal amplitude of the $^1O_2$ Stokes signal. Defining the efficiency as the relation between the number of photogenerated $^1O_2$ molecules divided by the number of pumping photons, we determine an efficiency of (8±2) 10^{-4} for H_2O at 410 nm. We compare the Raman method with the photosensitization method using Rose Bengal as a photosensitizer. The photosensitizer generates $^1O_2$ molecules rapidly, but the process eventually stops due to photobleaching of the photosensitizer. The Raman method generates $^1O_2$ molecules at a rate slower than the photosensitization methods. However, thanks to the intrinsic absence of photobleaching, the Raman method generates more $^1O_2$ molecules over time than the photosensitization method, despite its low efficiency values. The efficiency of the Raman method can be enhanced based on the fundamental principles of Raman interaction. Raman lasers, Raman amplifiers, and Raman fiber sensors are based on these principles [23-25]. Stokes signal grows exponentially with distance. The gain depends on the pumping field intensity, the nonlinear Raman susceptibility, and the propagation losses. A system should be designed to provide a significant gain for the $^1O_2$ Stokes component with low losses, while maintaining low gain and substantial losses for the solvent Stokes components. These considerations may play a crucial role in improving the $^1O_2$ Raman photogeneration efficiency for practical applications of the Raman approach. One useful application is the purification of water caused by viruses or bacteria. In a previous communication, we demonstrated the deactivation of viruses in an aqueous environment through simple irradiation with blue light, without the use of photosensitizers [26].

Funding: The research was sponsored by the Air Force Office of Scientific Research and was accomplished under Grant Number W911NF-23-1-0245. The views and conclusions are those of the author and should not be interpreted as representing the official policies, either expressed or implied, of the Air Force Office of Scientific Research or the US Government. The US Government is authorized to reproduce and distribute reprints for Government purposes, notwithstanding any copyright notation herein.

Data Availability Statement: Al relevant data are within the paper.

 doi:10.20944/preprints202507.2572.v1

Conflicts of Interest: "The author declares no conflicts of interest."

References

1. *Singlet Oxygen: Applications in Biosciences and Nanosciences, Volume 2 - Comprehensive Series in Photochemical & Photobiological Sciences*, Volume 14, 1st ed.; S. Nonell, C. Flors, editors. Cambridge, UK: Royal Society of Chemistry, Thomas Graham House, 2016.
2. Pibiri, I.; Buscemi, S.; Palumbo Piccionello, A.; Pace, A. Photochemically Produced Singlet Oxygen: Applications and Perspectives. *ChemPhotoChem* **2018**. 2(7), 535-547. https://doi.org/10.1002/cptc.201800076.
3. DeRosa, M.C.; Crutchley, R.J. Photosensitized Singlet Oxygen and its Applications. *Coordination Chem. Rev*. **2002**. 233-234, 351-371. https://doi.org/10.1016/S0010-8545(02)00034-6.
4. Sobotta, L.; Skupin-Mrugalska, P.; Mielcarek, J.; Goslinski, T.; Balzarini, J. Photosensitizers Mediated Photodynamic Inactivation against Virus Particles. *Mini Rev. Med. Chem*. **2015**. *15(6)*, 503-521.
5. Dougherty, T.J.; Gomer, C.J.; Henderson, B.W.; Jori, G.; Kessel, D.; Korbelik, M.; Moan, J.; Peng, Q. "Photodynamic Therapy". *JNCI: J. Nat. Cancer Inst*. **1998**. 90 (12), 889-905. http://dx.doi.org/10.1093/jnci/90.12.889.
6. Frank Kino, F.; Medeiros Silva, G.T. The Photophysics of Photosensitization: A brief overview. *J. Photochem. Photobiol.* **2021**. 7, 100042, https://doi.org/10.1016/j.jpap.2021.100042.
7. Michelin, C.; Hoffmann, N. Photosensitization and Photocatalysis - Perspectives in organic Chemistry. *ACS Catal*. **2018**. 8, 12046-12055.
8. Marcano Olaizola, A.; Kingsley, D.; Kuis, R.; A. Johnson, A. Stimulated Raman Generation of Aqueous Singlet Oxygen without Photosensitizers. *J. Photochem. Photobio. B: Bio* **2022**. 235, 112562. https://doi.org/10.1016/j.jphotobiol.2022.112562.
9. Marcano Olaizola, A.; Zerrad, A.; Jenneto, F.; Kingsley, D. "Confirming the Stimulated Raman Origin of Singlet-Oxygen Photogeneration". *J. Raman Spectros*. **2024**. 55, 58-64. https://doi.org/10.1002/jrs.6615.
10. Marcano Olaizola, A. "Near-Infrared Phosphorescence of Raman Photogenerated Singlet Oxygen." *Photochem* **2025**. 5(1), 7-14. https://doi.org/10.3390/photochem5010007.
11. Wilkinson, F.; Helman, W.P; Ross, A.B. Quantum Yields for the Photosensitized Formation of the Lowest Electronically Excited Singlet State of Molecular Oxygen in Solution. J. Phys. Chem. Ref. Data, **1993**. 22(1), 113-262.
12. Ossola, R.; Jönsson, O.M.; Moor, K.; McNeill, K. Singlet Oxygen quantum yields in environmental waters. *Chem. Rev.* **2021**, 121, 4100-4146. https://doi.org/10.1021/acs.chemrev.0c00781.
13. Lutkus, L.V.; Rickenbach, S.S.; McCormick T.M. Singlet Oxygen Quantum Yields Determined by Oxygen Consumption. *J. Photochem Photobiol. A: Chemistry*. **2019**. 378, 131-135. https://doi.org/10.1016/j.jphotochem.2019.04.029.
14. Morgan, J.; Yun, Y.J.; Ayitou A.J.L. Estimation of Singlet Oxygen Quantum Yield Using Novel Green-Absorbing Baird-Type Aromatic Photosensitizers. *Photochem. Photobiol*. **2022**. 98, 57-61.
15. Szewczyk, G.; Mokrzynski, K. Concentration-Dependent Photoproduction of Singlet Oxygen by Common Photosensitizers. *Mol.* **2025**. 30(5), 1130. https://doi.org/10.3390/molecules30051130.
16. Murasecco-Suardi, P.; Gassmann, E.; Braun, A.M.; Oliveros, E. Determination of the Quantum Yield of Intersystem crossing of Rose Bengal. Helvetica, **1987**. 70, 1760-1773. https://doi.org/10.1002/hlca.19870700712.
17. Salasi, M.; Pojtanabuntoeng, T.; S. Wong, S.; Lehmann, M. Efficacy of bisulfite ions as an oxygen scavenger in monoethylene glycol (at least 20 wt%)/water mixtures. *SPE J.* **2017**. 22(05), 1467–1477.
18. R. C. Trivedi, L. Rebar, K. Desal, L. J. Stong, New ultraviolet (340 nm) method for essay of uric acid in serum or plasma. *Clin. Chem*. **1978**. 24, 562-566.
19. F. Fisher, G. Graschew, H. J. Sinn, W. Maier-Borst, W. J. Lorenz, P. M, Schlag, A chemical dosimeter for the determination of photodynamic activity of photosensitizers. *Clin. Chim. Acta* **1998.** 274, 89-104.
20. Gao, Y.; Gong, N.; Sun, C.; Wang, W.; Men, Z. Stimulated Raman scattering investigation of isotopic substitution H_2O/D_2O system. *J. Mol. Liquids* **2020**. 297,11923.
21. Sun, Q. The Raman OH stretching bands of liquid water. *Vibrational Spectros*. **2009**. 51(2), 213-217.

 doi:10.20944/preprints202507.2572.v1

22. Bertie, J.E.; Lan, Z. Infrared intensities of liquids XX: The intensity of the OH stretching band of liquid water revisited, and the best current values of the optical constants of H_2O(l) at 25°C between 15,000 and 1 cm^{-1}," *Appl. Spectrosc*. **1996**. 50, 1047-1057.
23. Ozdal, B.; Bahram, J. Demonstration of a Silicon Raman Laser. *Opt. Exp*. **2004**. 12, 5269-5273. https://doi.org/10.1364/OPEX.12.005269.
24. Rong, H.; Jone, R.; Liu, A.; Cohen, O.; Hak, D.; Fang, A.; Paniccia, M. A Continuous -Wave Raman Silicon Laser. *Nature* **2005**. 433, 725-728. https://doi.org/10.1038/nature03346.
25. Guo, L.; Huang, J.; Chen, Y.; Zhang,B.; Ji, M. Fiber-Enhanced Stimulated Raman Scattering and Sensitive Detection of Dilute Solutions. *Biosensors* **2022**. 12, 243-254.
26. Kingsley, D.H.; Kuis, R.; Perez, R.; Basaldua, I.; Burkins, P.; Marcano Olaizola, A.; Johnson, A. Oxygen-dependent laser inactivation of murine norovirus using visible light lasers. *Virology Journal* **2018**. 15:117. https://doi.org/10.1186/s12985-018-1019-2.